APPLIED PHYSICS LETTERS 104, 000000 (2014)

Improvement of micro-bubble sizing using multi-harmonic excitations under the transducer bandwidth constraint

Damien Fouan,[1] Younes Achaoui,[2] and Serge Mensah[2]
[1]BF SYSTEMES, Technopole de la Mer, 229 chemin de la Farlède, 83500 La Seyne-sur-Mer, France
[2]Laboratoire de Mecanique et d'Acoustique, Universite d'Aix-Marseille and CNRS, 31 chemin Joseph Aiguier, 13420 Marseille, France

(Received 22 October 2013; accepted 15 January 2014; published online xx xx xxxx)

A microbubble sizing method based on the use of the odd harmonics of square-like excitations is presented. The microbubble resonance signature is determined by measuring the backscattered signals using the Dual Frequency Method combined with a time-frequency representation. The efficiency and the limitations of this method are described in the case of sine-like excitations. It is then established that the harmonics of square-like excitations can be used to significantly enlarge the range of microbubble detection and sizing. These findings were confirmed and explained by theoretical studies on microbubble dynamics based on the Keller-Miksis formulation. © 2014 AIP Publishing LLC. [http://dx.doi.org/10.1063/1.4868654]

Measuring microbubbles' size distributions in multiphasic media is still a crucial issue in fields such as oceanology, biology, medicine, and industry (nuclear reactors). During exposure to hyperbaric decompression as in diving and hyperbaric medical procedures, both the absolute ambient and the absolute inspired pressures decrease and small bubbles (10–700 lm)[1] may develop from pre-existing gas nuclei (0.1–5 lm) present in tissue.[2] These micro-bubbles constitute a potential risk to subjects such as divers[3] and astronauts,[4] since they can result in severe diseases such as joint pain and neurological manifestations.[5] Information about the size, density, and at least the existence of bubbles in liquids and solids are usually processed using optical or acoustical methods. Although photographic and holographic methods give high-resolution images, they are useless in the case of opaque media where acoustical methods are therefore more suitable.

Several methods of detecting, sizing, and estimating bubble populations have been developed during the last four decades in order to prevent decompression sickness. For example, the presence of micro-bubbles can be detected using the classical B-mode imaging method[6] or with the widely used Doppler systems.[7] The latter systems can be used to clearly distinguish the signals backscattered by stationary tissues and microbubbles circulating in blood. However, they can be applied exclusively to bubbles in motion, and these methods provide no information about the bubble size. In addition, Doppler signals require a trained ear to interpret even approximately the amount of bubbles passing through the right ventricle.[7]

In 1985, Chapelon et al. developed the Dual Frequency Ultrasound Method based on the simultaneous insonification of low and high frequency ultrasound waves.[8] A frequency modulation is applied to the low frequency (LF) wave, the spectral band of which covers the resonance frequency range of the bubble to be sized. The high frequency backscattered wave is modulated by the microbubble cross-section, the amplitude of which increases when the bubble is resonating. The micro-bubble radius can therefore be calculated by applying Minnaert's formula.[9] This approach has proved to be efficient when applied to stationary bubbles in tissues.[10,11] In the case of moving bubbles in blood, the range of radii involved is known to be much larger. For this technique to be applicable to circulating bubbles, the following requirement has to be fulfilled.

The measurements should be performed within a very short time. The time during which microbubbles can be assumed to pass through the acoustical field has been estimated at 20 to 50 ms, depending on the stage in the cardiac cycle.[12] These measurements therefore have to take less than 10 ms. This makes it possible to average successive responses originating from the same bubble. Previous studies on the Dual Frequency Method have not dealt with practical issues of this kind, since they focused on the feasibility of the method on almost stationary bubbles. In this Letter, we extend the use of the Dual Frequency Method to a larger range of bubble radii, thanks to the use of non-sinusoidal excitations. Since bubbles are sensitive to both the fundamental component and the excited harmonics, the use of suitably chosen chirped non-sinusoidal excitations adapted to the transducer bandwidth makes it possible to characterize a large population of microbubbles passing through the right ventricular.

Since the mass density of water and blood are almost identical, and dumping due to viscosity does not affect the resonance frequency in the case of large bubbles,[13,14] the experiments described in this paper were performed in water. We therefore used a 2 m 3 m water tank in order to reduce standing wave effects. Micro-bubbles ranging between 20 lm and 200 lm in size were produced in this tank by a hydrojet (Braun OralB). A thin wire was placed on the path of the rising bubbles, and measurements were performed on a single tethered bubble (Figure 1(a)). Using this simple method, several measurements were carried out under practically the same conditions and compared. The micro-bubble radius was assumed to be constant during the 100-ms duration of the measurement. The acoustically characterized bubbles were monitored optically at the same time by means of a CCD camera. The acoustic measurements were performed using three confocused transducers. The first transducer

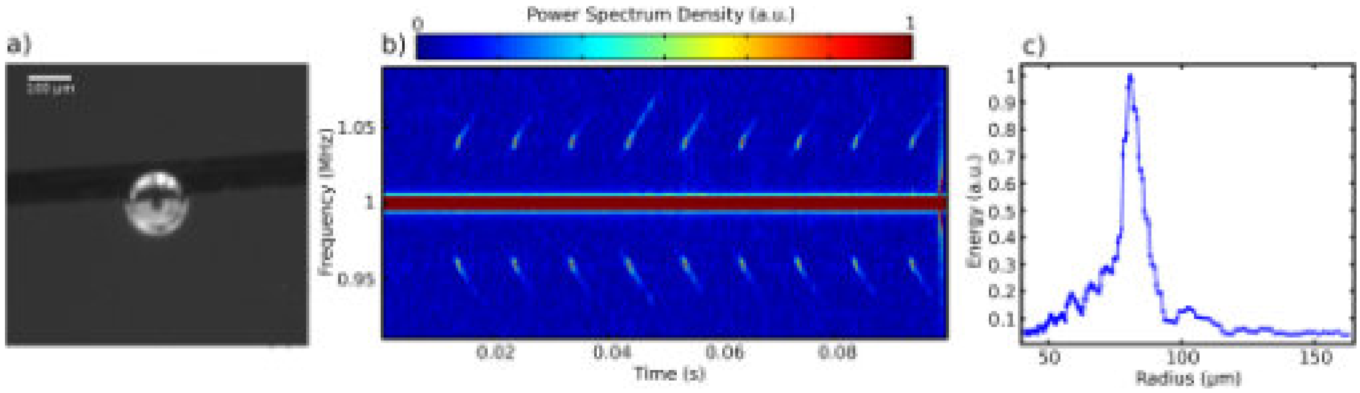

FIG. 1. (a) A 81-lm bubble photographed with a CCD camera, (b) TF spectrogram of the imaged bubble, and (c) average cross section of the ten measurements calculated from the TF spectrogram.

radiated the LF pumping wave (Ultran, GMP 50 kHz; [35–70] kHz bandwidth), and the other two were responsible for the emission and reception of the imaging wave (Imasonic, 1 MHz, f ¼90 mm). The two emitting transducers were connected to an arbitrary waveform generator (LeCroy, ArbStudio 1104, four channels). The receiving transducer was connected to an oscilloscope (Agilent Technologies, Infini-iVision DSO5014A, 100 MHz).

Since the exact size of the microbubble to be characterized was assumed to be unknown, the consecutive pumping waves were replaced by sweeps in order to size bubbles with a radius ranging between 55 lm and 110 lm in radius. The corresponding resonance frequencies amounted to 60 and 30 kHz, respectively. The imaging wave was continuous, and its frequency f_i was kept at 1 MHz. The transmitted acoustic power applied should be as low as possible, especially at low frequencies, in order to avoid newly developing microbubbles from cavitation and biological damage from occurring in saturated media.[14] The voltage of both signals was therefore set at 12 V pp, resulting in pressure levels of 10 kPa and 500 Pa at the focal point in the case of high and low frequency waves, respectively. Automated recordings processed 10 sweeps at a time, and the results were displayed in a Time-Frequency (TF)-diagram (Figure 1(b)). It is worth noting that the chirp rate depended on the length of the sweep. As explained below, this slope is one of the key parameters for obtaining accurate microbubble sizes. In the TF-diagram (Figure 1(b)), the maximum amplitude of the backscattered modulated waves was observed at 160.0395 MHz. The exact size of the tethered microbubbles was determined by averaging the TF-profiles and applying the Minneart formula (Figure 1(c)). The correspondence between the acoustical and optical data is presented in Figure 1(c), taking the 2.3-lm optical resolution of the camera into account.

Several measurements were then performed in order to determine the signal to-noise-ratio of broadband excitations versus the time sweep duration. The resulting signal-to-noise ratios obtained on 5 different bubbles with sizes of around 80-lm measured 8 times each are presented in Figure 2. With the bubbles under investigation, the effects of the chirp rate were found to be negligible at frequencies of less than 5kHz/ms. Beyond 25 kHz/ms, the detection became practically impossible since we reached the noise level. Between these two values, the signal magnitude lost around 1 dB every 3.5 kHz/ms. In order to identify a broad range of bubble radii in the right ventricle within the time depending on, the sine-like method of excitation is no longer suitable since voluminous bubbles take a longer time to oscillate. It was therefore proposed to compare the cases of two bubbles differing significantly in size (62 lm and 15 lm) under the sine-like and square-like conditions of excitation. AQ1

For this purpose, simulations were performed omitting the transducer bandwidth information with a view to describing the bubbles' dynamics. Time-dependent changes in the bubble radius were then calculated using the Keller-Miksis equation combined with thermal damping terms based on Eller's model.[15,16] The dynamic response of the 62-lm bubble excited by a sine-like [10–300 kHz]-chirped signal is presented in Figures 3(a) and 3(b) where it can be seen that the maximum energy of about 2% corresponds to a resonance frequency of approximately 52 kHz. The signature of the bubble's non-linearity can also be identified at twice the component resonance frequency (Figure 3(a)). The square-like [10–90kHz]-chirped signal subsequently applied in order to make comparisons with the former case is presented in the form of three sine-like signals, namely, [10–90 kHz], [30–270kHz], and [50–450 kHz], taking the corresponding Fourier coefficients into account (Figures 3(c) and 3(d)). The TF-diagram in Figure 3(c) shows the enhancement of both

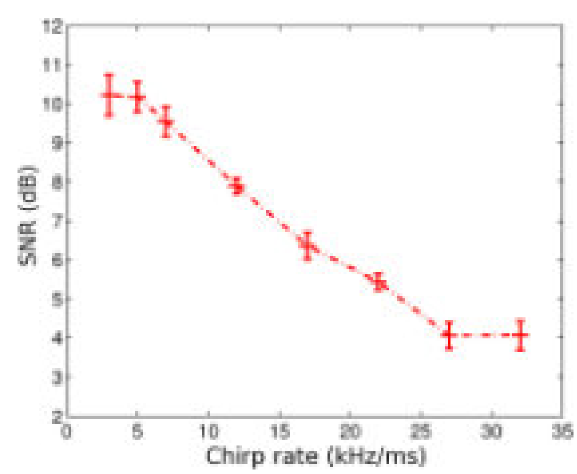

FIG. 2. Signal to noise ratio of the classical method versus TF sweep slope.

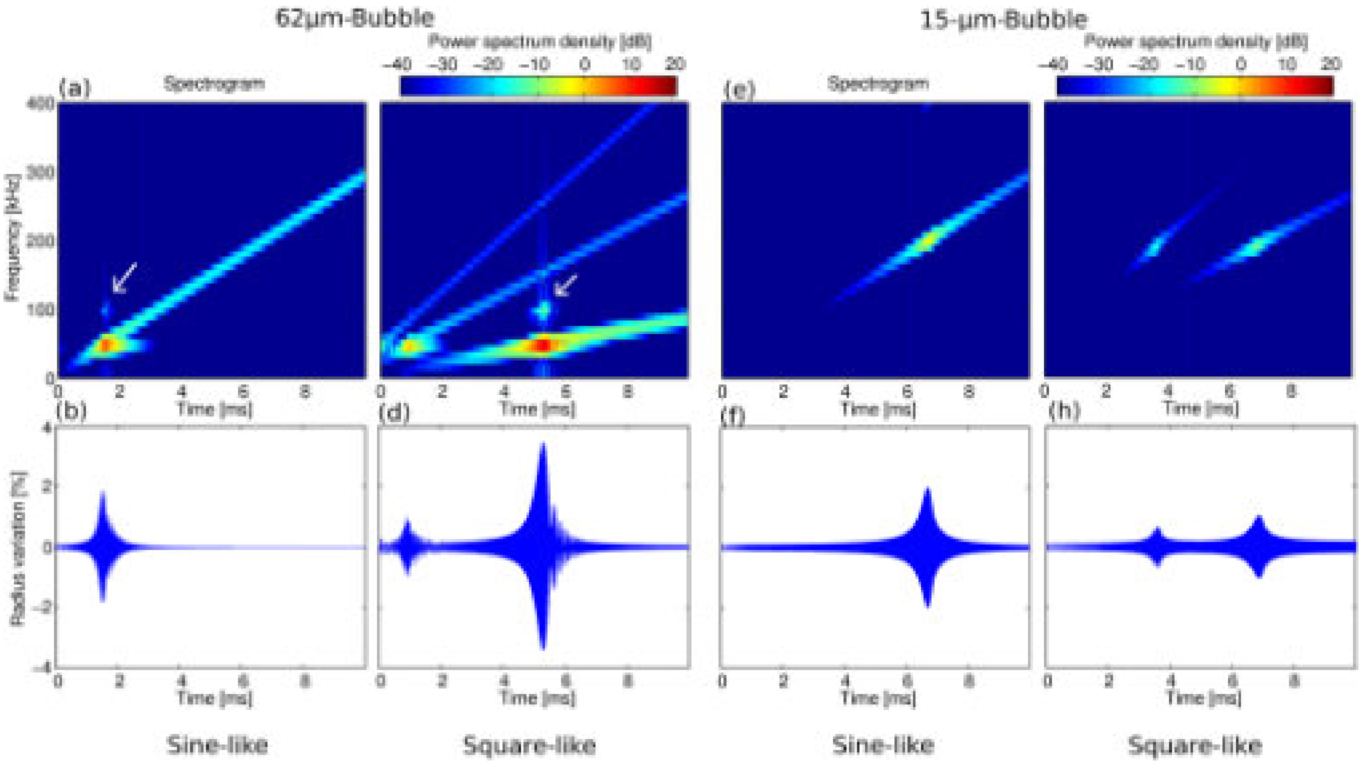

FIG. 3. (a) Theoretical TF diagram obtained with the 62-lm-bubble using a [10–300kHz]-sine-like chirp. (b) Time-dependant bubble response corresponding to (a). (c) and (d) as in (a) and (b) in the case of [10–90kHz]-square-like excitation. (e), (f), (g), and (h) are, respectively, the exact equivalent of (a), (b), (c), and (d), respectively, in the case of a 15-lm-bubble. The white arrows indicate the second harmonic due to the non-linearity of the bubble in order to avoid any confusion with the excitations harmonics. In all the theoretical part, the pressure value was set to 500Pa.

the fundamental dynamic response of the bubble and the second harmonic due to non-linearity. The time related changes in the radius variation in Figure 3(d) faithfully reflect the amplification of the resonance by a factor of almost two. In addition, the strategy presented here gives the multiple detection from the third harmonic in the [30–270 kHz] frequency range and more imperceptibly, the fifth harmonic [50–450 kHz]. Simulations of sine-like and square-like excitations applied to tiny bubbles are presented in Figures 3(e)–3(h). As in the previous case, the TF-diagrams clearly show the resonance frequency of such bubble around 210 kHz under both sine-like and square-like excitation. Although the detection can be monitored by the third and fifth harmonics of the square-like signal, the sine-like signal is more suitable for these tiny bubbles, since the fundamental of the square-like excitation cannot reach this frequency.

In order to specify the range sin which each excitation is suitable, we performed a series of simulations of a number of bubbles ranging from 5 lm to 150 lm in size. Figure 4(a) gives the relative changes versus the radius under both sine-like and square like excitations for the sake of comparison. These results show that below radii of 20 lm, the sine-like excitation describes the dynamics of the bubble better than the third and fifth harmonics (below 12 lm) of the square-like excitation. This is obviously due to the Fourier coefficients. However, because of the low chirp rate, the detection of voluminous bubbles is noticeably enhanced. Since the latter bubbles are more dangerous during decompression sickness, the priority of the method is to detect these microbubbles accurately. In more concrete situations where the transducer bandwidth and the noise level are inevitable and therefore have to be taken on board, a suitable choice of swept square signal would result on the detection of further tiny bubbles. As shown in Figure 4(b), tiny bubbles are easily detectable since their resonance frequency falls within the 250 kHz-transducer bandwidth. In addition, large bubbles whose the frequency resonance lied outside the transducer bandwidth were quite detectable.

Based on these theoretical results, tethered or moving bubbles will predictably vibrate under the Fourier harmonics

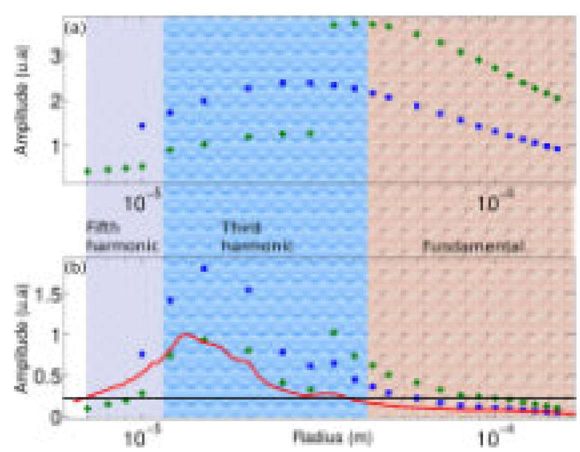

FIG. 4. Maximum amplitude recorded from the time bubble response versus the bubble radius using the [10–300kHz]-sine-like (blue cross) and [10–90kHz]-square-like (green plus) excitations, (a) without and (b) taking into account the 250kHz-transducer bandwidth. The red and black lines represent the exact 250kHz-transducer bandwidth and the noise level estimated in the experiments, respectively. The figure was colored to highlight which harmonic takes the control of the process when using the [10–90kHz]-square-like signal.

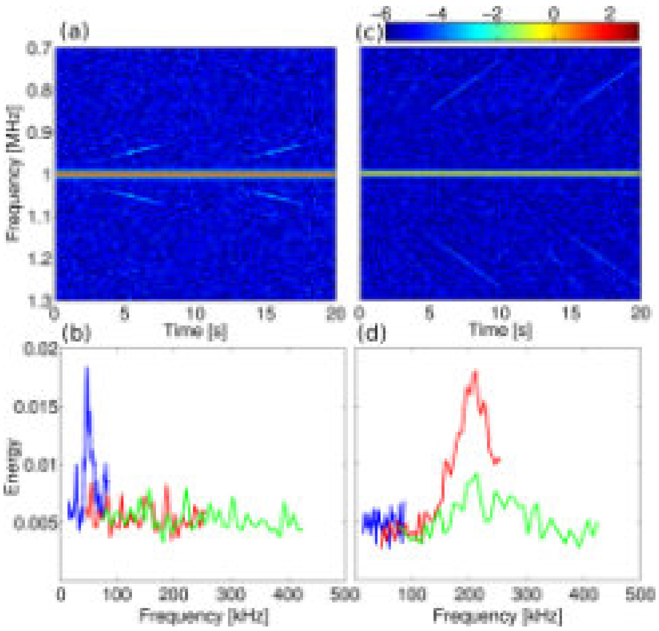

FIG. 5. (a) Experimental TF-diagram obtained for the 62-lm-bubble using the [10–90kHz]-square-like excitation using the 250kHz-transducer. (b) Average cross section of the ten measurements calculated from the TF-diagram. The blue, red, and green lines represent the fundamental, the third, and the fifth harmonics, respectively. (c) and (d) as (a) and (b) in the case15-lm-bubble.

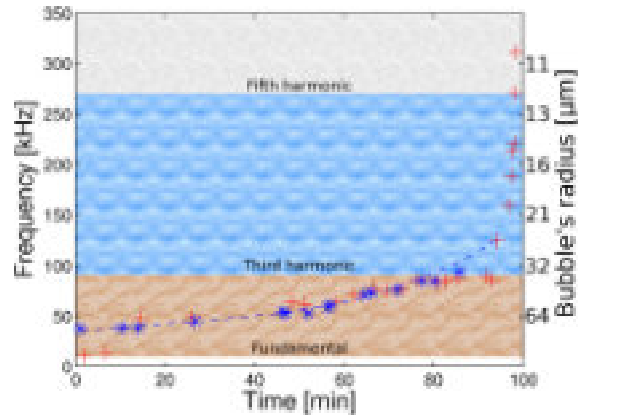

FIG. 6. Characterization of a 78-lm bubble diffusion process, taking full advantage of the [10–90kHz]-square-like excitation (red pluses) using a 250kHz-transducer. The blue stars give the reference values obtained using the [10–150kHz]-sine-like chirped wave radiated by a 50-kHz transducer.

of a non-sinusoidal periodic signal as long as they communicate enough energy. We therefore carried out experimental investigations on the two former bubble radii, namely, 62-lm and 15-lm bubbles under square-like excitations using the 250 kHz-transducer [200–300] kHz bandwidth. In the TF-diagram presented in Figure 5(a), the fundamental slope can be observed near the resonance frequency. The resonance frequency of the 62-lm-tethered bubble was determined by averaging the TF-profiles (Figure 5(b): the blue, red, and green lines represent the fundamental, the third and fifth harmonics, respectively). Because of the low values of the Fourier coefficients and the weak electromechanical conversion by the transducer near the resonance frequency (52kHz), the bubble could not be distinguished from the noise level (red and green lines). However, the insonification of the 15-lm-tethered bubble gave no responses in the fundamental sweep (blue line) since the resonance frequency of the bubble is out of it. The third and fifth harmonics, therefore, took the control of the process (red and green lines, respectively). The frequency corresponding to these resonances was 208 kHz, which corresponds to a 15.4-lm resonant bubble.

Lastly, 26 measurements were conducted on a 78-lm bubble dissolving in undersaturated water during the well-known natural diffusion process.[17] Figure 5, which summarizes this process, shows that the bubble could be sized down to a radius of 9lm. These measurements were performed in two steps. Measurements based on sine-like excitations were first performed using the 50-kHz transducer, taking advantage of its bandwidth while exciting the bubble with the [10–90kHz] chirped signal used. Values marked with blue stars describing the evolution of the bubble diffusion process were used as reference values. The 50-kHz transducer was then replaced by the 250-kHz one and measurements were carried out with [10–90kHz]-square-like signals. It is worth noting that the values recorded between 15 and 85 nm] AQ2
match the reference values quasi-perfectly. In addition, the micro-bubble could still be sized up to a radius of 98 nm, and the final size detected corresponded to a 9-lm-bubble. The two discrepancies observed at around 5 and 95 min were due to the noise and to the lower and upper limits of the [10–90 kHz] excitation, respectively.

In conclusion, square-like excitations can be used to size microbubbles using the Dual Frequency Method and time-frequency diagrams in a wide range of radii. This extension of the method was made possible by lowering the fundamental component chirp rate in order to cope with the inertia associated with large bubbles. The odd harmonics make it possible to deliver at the same time a suitable level of energy for exciting down to six times smaller bubbles. These results can be improved by carefully taking the transducer bandwidth into account, using non-linear frequency sweeps such as exponential modulations (Figure 6). AQ3

This work was partly supported by the French Research Ministry under the Smart US project, Ref. ANR-10-BLAN-0311, the Provence-Alpes-Cote-d'Azur Council, in the framework of the Comedies project, the PACA Canceropole and the French Ministry of Defense under the BORA project.

[1]B. A. Hills and B. D. Butler, Undersea Biomed. Res. 8(3), 163 (1981). AQ5
[2]T. R. Hennessy, in International Symposium on Supersaturation and Bubbles Formation in Fluid-Sand Organism (1989).
[3]R. D. Vann, F. K. Butler, S. J. Mitchell, and R. E. Moon, The Lancet 377, 153–164 (2011).
[4]R. Y. Nishi and and P. J. Sullivan, in First Panel on U.S./Japan Diving Physiology, Technology and Aerospace Medicine (UJNR) (2000).
[5]T. J. Francis and S. J. Mitchell, Pathophysiology of Decompression Sickness (Elsevier, 2004), pp. 165–183. AQ4
[6]O. S. Eftedal and A. O. Brubakk, Med. Biol. Eng. Comput. 31, 627–633 (1993).
[7]K. Kisman, Ultrasonics 15, 105–110 (1977).
[8]J. Y. Chapelon, P. M. Shankar, and V. L. Newhouse, J. Acoust. Soc. Am. 78(1), 196–201 (1985).
[9]M. Minnaert, Philos. Mag. Series 7 16(104), 235–248 (1933).
[10]J. C. Buckey, D. A. Knaus, D. L. Alvarenga, M. A. Kenton, and P. J. Magari, Acta Astronaut. 56(9–12), 1041–1047 (2005).

[11]B. R. Bollinger, J. C. Wilbur, T. G. Donoghue, S. D. Phillips, D. A. Knaus, P. J. Magari, D. L. Alvarenga, and J. C. Buckey, Undersea Hyperbaric Med. 36(2), 127–136 (2009).
[12]K. D. Horton, R. W. Meece, and J. C. Hill, J. Am. Soc. Echocardiogr. 22, 776–792 (2009).
[13]D. B. Khismatullin, J. Acoust. Soc. Am. 116, 1463 (2004).
[14]R. E. Apfel and C. K. Hollad, Ultrasound Med. Biol. 17, 179–185 (1991). AQ6
[15]J. B. Keller and M. Miksis, J. Acoust. Soc. Am. 68, 628 (1980).
[16]A. I. Eller, J. Acoust. Soc. Am. 47(5B), 1469–1470 (1970).
[17]P. S. Epstein and M. S. Plesset, J. Chem. Phys. 18, 1505 (1950).